Proceedings of ISFOG 2025
5TH INTERNATIONAL SYMPOSIUM ON
FRONTIERS IN OFFSHORE GEOTECHNICS
Nantes, France | June 9-13 2025

ISBN 978-2-85782-758-0

Field test to investigate the cyclic tensile response of open-ended piles installed in sand

A. Sharma, A. Peccin da Silva*, D. de Lange
Deltares, Delft, Netherlands

Y. Jafarian
Seaway7, Zoetermeer, Netherlands, formerly Deltares, Delft, Netherlands

K.G. Gavin
TU Delft / InGEO Consulting, Delft, Netherlands

J. Kenkhuis
Bluewater Energy Services, Hoofddorp, Netherlands

anderson.peccindasilva@deltares.nl (corresponding author)

ABSTRACT: As the global transition to renewable energy accelerates, ensuring the reliability of foundations in offshore structures is increasingly important. In the context of floating wind structures, pile foundations can be used as anchor points for station keeping against significant cyclic loading. Tubular piles have proven reliable while offering a high tensile load capacity, but accurate predictions of pile tensile capacity and stability without extensive testing are essential to avoid over-conservative design. This paper presents findings from the Tubular Pile Pull-out Testing (TPPT) Joint Industry Project, which involved field testing on tubular steel piles under monotonic and multi-stage cyclic loading at the Port of Rotterdam. This paper primarily discusses the comparison between predicted and measured pile capacity and stability under cyclic loading. The predictions were based on interaction charts recommended in the literature for piles under tensile loading. Pile responses in interaction charts are classified as stable, metastable, or unstable based on their displacement responses to the applied cyclic loading in relation to the static capacity. The results observed in the field tests are compared with the stability response previously defined in the literature. In particular, the TPPT testing programme included tests near the chart zone where stable and metastable curves converge towards the unstable zone, where the proximity between curves leads to uncertainties in determining pile stability.

Keywords: pile, tensile capacity, cyclic loading, load interaction charts, floating wind turbine foundation.

1 INTRODUCTION

In the context of offshore renewable energy, open-ended steel piles are often used to support wind turbines. While for bottom fixed-structures the (mono) piles are subjected to predominantly lateral loads, for floating wind turbines anchor piles experience axial tensile cyclic loading in service. The same applies to jacket bottom-fixed structures. Recently, Lehane et al. (2020) developed the unified CPT-Based Method design approach included in the latest ISO design code. The method is used to predict the pile capacity design under axial (compressive and tensile) monotonic loading. The method does not account for cyclic loading. Further understanding of the cyclic response of anchor piles is particularly important for mooring tension-leg platforms (TLPs), for which the cost of the foundation is significant due to the larger loads in comparison with other mooring configurations such as catenary lines connected to semi-submersible floaters.

In that context, full-scale tests were conducted on four open-ended steel piles at the Port of Rotterdam (Maasvlakte 2) as part of the JIP *"Tubular Pile Pull-out Testing (TPPT)"*. The piles were subjected to static and cyclic loading under different load levels and the displacement during each loading stage was recorded.

This paper presents the results of the cyclic tests in terms of pile stability for each cyclic package and amplitude and how the results compare with Load Interaction Charts previously proposed in the literature.

2 BACKGROUND

2.1 Nomenclature for cyclic loading

Cyclic loading episodes can be defined in terms of Q_{cyclic} and Q_{mean}, where Q_{mean} is the mean load and Q_{cyclic} is the load amplitude between the mean load value and

the maximum load applied. Both are related to the maximum and minimum values of the load, Q_{max} and Q_{min}, respectively, as illustrated in Figure 1.

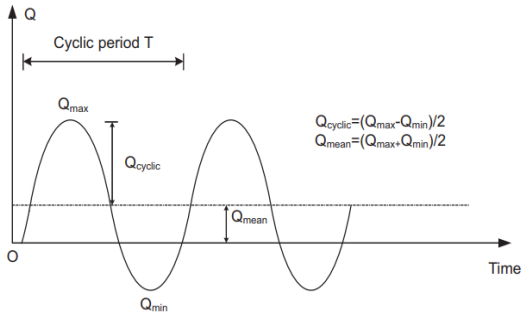

Figure 1 Cyclic loading nomenclature (Tsuha et al., 2012).

2.2 Load interaction charts and pile stability

Axial cyclic load interaction charts were introduced by Jardine & Standing (2012) based on tests executed in Dunkirk, France. These differentiate the stability of the pile into three zones: stable, metastable, and unstable, see Figure 2 – solid lines. The axes represent Q_{mean} and Q_{cyclic} values (as defined in section 2.1) normalised by the static load capacity Q_{max_static}.

The response of the pile is classified based on the accumulation of displacement in relation to the number of cycles N. Interaction charts are employed to predict this response in advance. The definitions of these pile responses, in terms of displacement behaviour, are outlined below, as defined by Jardine & Standing (2012):

- Stable (S): Pile head displacements accumulate slowly over hundreds of cycles.
- Unstable (US): displacements develop rapidly under one-way or two-way conditions leading to failure at N<100 and marked shaft capacity losses.
- Metastable (MS): pile head displacements accumulate at moderate rates over tens to hundreds of cycles without stabilising and cyclic failure develops within the 100<N<1000 range.

More recently, Igoe & Gavin (2021) proposed new stability zones for the load interaction charts, see Figure 2 based on field tests carried out with steel tubular piles in sands at the Blessington testing site in Ireland. It is worth noting the differences in testing conditions between the Dunkirk and the Blessington sites. In the Dunkirk, most piles had around 19 m in embedded length with the ground water table at around 4 m depth. The loading frequency was between 0.017 Hz and 0.0083 Hz. For the Blessington tests, the piles had 7 m of embedded length, and the water table was well below the tip of the piles. The loading frequency was 0.1 Hz.

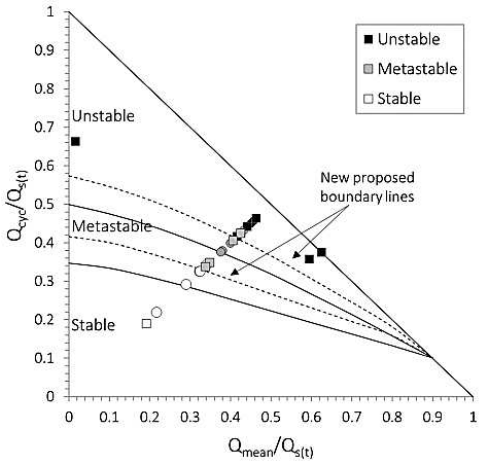

Figure 2 New boundaries for load interaction charts proposed by Igoe & Gavin (2021) in comparison with the boundaries of Jardine & Standing (2012).

2.3 Consideration of pile ageing

Pile ageing is a known phenomenon by which the pile increases in capacity with time (Gavin et al. 2015). In the load interaction charts of Jardine & Standing (2012), the pile capacity at a given time was calculated based on the ICP-05 method (Jardine et al. 2005), and an ageing factor was applied to consider the change in capacity with time. Igoe & Gavin (2021) used measured pile capacities with time. Therefore, in both load interaction charts the pile static capacity includes an ageing factor to ensure the static capacity relates to the capacity at the time of cyclic loading.

Jardine et al. (2006) found that the ageing capacity of piles depends on their loading history. Intact piles, not subjected to any load since installation, develop a higher ageing factor compared to previously loaded piles. This difference is depicted in Figure 3, which presents the static capacity of piles at a time t ($Q_{s(t)}$) in relation to the pile capacity calculated by the ICP method ($Q_{s,\,ICP}$), as a function of time after installation.

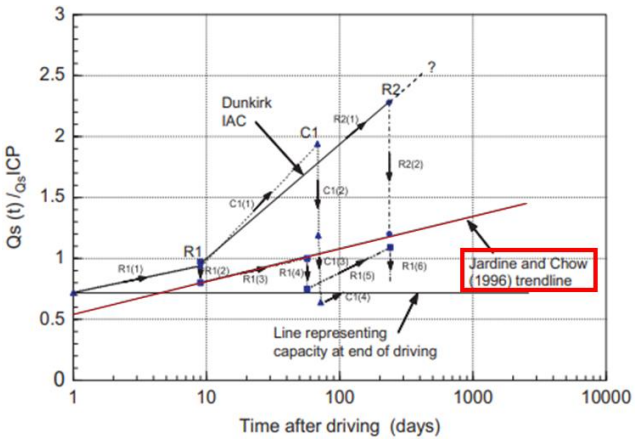

Figure 3 Ageing effects for pile capacity as a function time after driving (Jardine et al., 2006)

In this paper, the ageing line of Jardine & Chow (1996) is selected since the piles subjected to tensile loading were previously subjected to static compressive loading, as will be explained in the next section.

3 FIELD TESTS

The test piles were installed at the Maasvlakte 2 part of the Port of Rotterdam, in The Netherlands. Prior to the test campaign, 3 Cone Penetration Tests (CPT) were executed on each of the 6 potential pile locations, from which 4 pile locations were selected.

More details regarding site characterization are presented hereafter.

3.1 CPT/ site characteristics

CPT tests were conducted before installation of all piles. CPT profiles taken near the location of Pile 1 are shown in Figure 4. These CPT results are also representative for the other pile locations.

The soil profile consisted of predominantly sand. The top 5 m consisted of sand fill, artificially deposited during the reclamation of the port area (2008-2015). The sand layers from 5 m to 11 m depth were deposited for the construction of a dredging depot (1986-1987). Silty, clayey and clean sand deposits from the Naaldwijk Formation are found from 11 m to 27 m depth. Below this, clay/peat layers from the Nieuwkoop Formation are found on top of the Pleistocene sand deposits which start from 30 m depth. The ground water level was 1.5 m to 2.5 m below ground due to tidal variations.

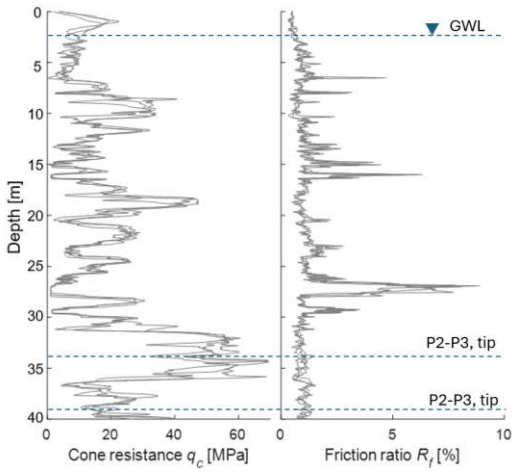

Figure 4 CPT for Pile 1, representative of the testing site

3.2 Pile dimensions and installation

The outer diameter of the piles was 1.22 m and the total length was ~ 34 m for Piles 2 and 3 and ~ 39 m for Piles 1 and 4. The wall thickness of the piles was predominantly 16 mm, with part of the pile near the surface having a larger thickness (17-19 mm) to meet the tensile testing requirements. Two piles were installed to a depth of 38.3 m, whereas the two shorter piles were installed to a depth of 33.3 m. The piles were first installed by vibratory pile driving up to about 29.8 m depth. Subsequently, the piles were impact driven to the final depth.

3.3 Pile loading

All piles were subjected to compression loading up to geotechnical failure (defined as a displacement of 10% of diameter) prior to the application of tensile loads, whose results are omitted from this paper for the sake of brevity. The waiting time between compressive and tension loading varied between 62 days (Pile 3) and 147 days (Pile 4).

The loads were measured using 6 calibrated load cells between the hydraulic jacks and the reaction beams. The pile head displacement was measured by 4 LVDTs (90° apart from each other) placed 0.50 cm above ground level and connected to reference beams (Figure 5). Total stations were used to measure any potential displacements of the reference beam, as well as a back-up for the pile head displacements.

Figure 5 Position of 2 LVDTs on the pile

The loading histories for piles 1, 2 and 4 under tension are presented in Table 1 through Table 3. The values presented in the tables are the predominant loads throughout the cyclic packages. The loads Q_{max} and Q_{min} sometimes varied within $\pm$ 10% of the values in the table. For the last cyclic package of Pile 2, this variation was larger, as seen in Figure 6. The same figure shows an example of the load history of one of the piles (Pile 2).

All cyclic loading was applied with a frequency of around 0.05 Hz, similar to the frequency applied in the tests of Igoe & Gavin (2021) and much higher than the frequency of Jardine & Standing (2012).

Table 1 Tension loading history for pile 1

Loading package	No. of cycles	Q_{min} (kN)	Q_{max} (kN)	Q_{mean} (kN)	Q_{cyc} (kN)
Cyclic 1	1000	3190	5110	4150	960
Cyclic 2	890	3400	6950	5175	1775
Cyclic 3	1000	3020	6300	4660	1640

Cyclic 4	1000	2760	7060	4910	2150

Table 2 Loading history for pile 2 under tension

Loading package	No. of cycles	Q_{min} (kN)	Q_{max} (kN)	Q_{mean} (kN)	Q_{cyc} (kN)
Cyclic 1	1000	1365	1880	1623	258
Cyclic 2	1000	850	3100	1975	1125
Cyclic 3	1000	1450	3830	2640	1190
Cyclic 4.1	1000	930	4700	2815	1885
Cyclic 4.2	1000	2470	4595	3533	1063
Cyclic 5	1000	4885	5420	5153	268
Cyclic 6	1000	4750	6050	5400	650

Table 3 Loading history for pile 4 under tension

Loading package	No. of cycles	Q_{min} (kN)	Q_{max} (kN)	Q_{mean} (kN)	Q_{cyc} (kN)
Cyclic 1	1000	3150	5300	4225	1075
Cyclic 2	1000	3450	6220	4835	1385
Cyclic 3	1000	2600	7100	4850	2250
Cyclic 4	1000	3430	7810	5620	2190

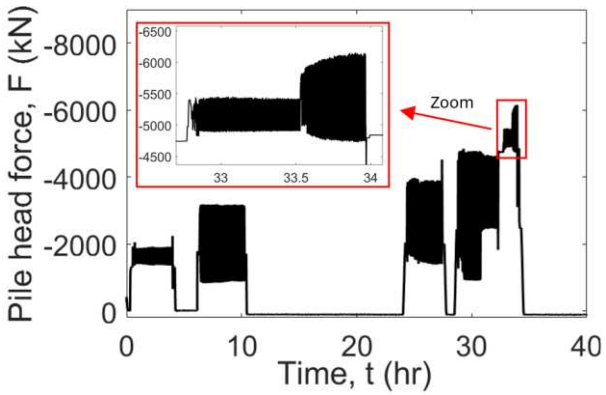

Figure 6 Example of pile loading history (Pile 2)

While Piles 1, 2, and 4 were subjected to tensile cyclic loading, Pile 3 was loaded statically in tension. The capacity of Pile 3 (taken as the load at which the vertical displacement at pile head reached 10% of the pile diameter) was 6909 kN. The load was increased in several steps with a load rate between 1.5 to 2.1 kN/s, after which the load was kept constant for at least 30 minutes, but up to 2.5 h for higher load levels. In addition to the measured static tensile capacity of Pile 3, the capacity of all the piles under tension was calculated using the Unified CPT Method, as summarized in Table 4. The differences in calculated pile capacities relate mainly to the different embedment lengths. Small differences between piles of same length (Piles 2-3 and Piles 1-4) relate to slight differences in soil profile and associated cone resistances at each pile location.

Table 4 Pile capacities calculated from the Unified CPT Method

Pile number	Calculated tensile capacity, $Q_{U\text{-}CPT}$ (kN)	Measured tensile capacity (kN)
1	6631	-
2	5557	-
3	5601	6909
4	6515	-

It is worth noting that the measured capacity of Pile 3 includes some effect of ageing, as the pile was loaded 134 days after installation, while the calculated capacity from the Unified CPT Method shown in Table 4 considers around 10-30 days between installation and loading (mean 14 days).

4 RESULTS & DISCUSSION

This section compares the pile stability response as observed from the accumulated displacements with the expected response based on load interaction charts. In order to place the cyclic loading packages in the interaction charts, the static capacity of each pile at the moment of testing (i.e. including ageing) must be determined, as well as the load amplitudes of each package. This is covered in the next sections.

4.1 Pile capacities accounting for ageing

Ageing was accounted for by using the trendline proposed by Jardine & Chow (1996), as previously shown in Figure 3. An ageing factor based on the number of days between pile installation and tensile loading was therefore applied to the capacity calculated from the Unified CPT Method ($Q_{U\text{-}CPT}$) to obtain the estimated static capacity at the time of cyclic loading ($Q_{s(t)}$). For the selection of the ageing factors, the time between compression tests and tensile tests is neglected which is recognised as an important simplification. The values of $Q_{s(t)}$ accounting for ageing, which are also used for the interaction charts, are presented in Table 5.

For Pile 3, a comparison can be made between the estimated pile capacity accounting for ageing and the actual measured capacity from the static tensile loading test. While the estimated capacity including ageing was 6385 kN, the measured capacity from the load test was 6909 kN, i.e. 8% larger.

Table 5 Estimated pile capacities at the time of loading accounting for ageing

Pile number	$Q_{U\text{-}CPT(14)}$ (kN)	Days instal. to loading	Ageing factor	$Q_{s(t)}$ (kN)
1	6631	159	1.16	7692
2	5557	147	1.15	6391
3	5601	134	1.14	6385
4	6515	175	1.17	7623

4.2 Pile stability during cyclic loading

The results for each cyclic loading package are classified into stable (S), metastable (MS) and unstable (US), based on the criteria previously described in section 2.2, and shown in Table 6 below. The stability

classifications highlighted in red identify the cases where the expected response according to the load interaction charts are different from the observed stability response based on the measured displacement accumulation in the field tests. It is worth noting that the interaction charts to which the comparison is made used piles of smaller diameters installed with a different method into different soil profiles, and loaded with different cyclic frequencies, hence the comparison is not aimed at verifying the accuracy of previous interaction charts, as different tests or sites are expected to provide different charts.

Table 6 Expected and observed pile stability for each cyclic loading package

Pile	Cyclic package	Q_{cyc} (kN)	Q_{mean} (kN)	Expected response(*)	Observed response
1	1	960	4150	S // S	S
1	2	1775	5175	US // MS	MS
1	3	1640	4660	MS // S	S
1	4	2150	4910	US // MS	MS
2	1	258	1623	S // S	S
2	2	1125	1975	S // S	S
2	3	1190	2640	S // S	S
2	4-1	1885	2815	MS // MS	MS
2	4-2	1063	3533	S // S	S
2	5	268	5153	S // S	S
2	6	650	5400	S // S	US
4	1	1075	4225	S // S	S
4	2	1385	4835	S // S	S
4	3	2250	4850	US // US	US
4	4	2190	5620	- // -	US

(*) Left: from Jardine & Standing (2012)'s boundaries; Right: from Igoe & Gavin (2021)'s boundaries

Figure 7 displays the load interaction chart for all cyclic packages of piles 1, 2, and 4. The initial comparison utilizes Jardine & Standing (2012)'s lines to separate stable, metastable, and unstable zones. Although overall a good agreement is observed, the points marked with red circles do not match with the observations made from the field test data. These points are just slightly above the proposed boundaries. Notably, one point (P4, cyclic 4) appears outside the line due to an atypical and irregular cyclic load, as the mean amplitude in this instance was continuously varying. Such cyclic loading is unsuitable for predictions made using interaction charts and should be disregarded in the analysis. In addition, for P4, cyclic package 6, Q_{cyc} is increasing significantly and loads closer to the capacity of the pile are applied in the end, as shown previously in Figure 6.

A similar comparison was conducted using the lines proposed by Igoe & Gavin as shown in Figure 8. The response observed in the field tests aligns more closely with the response predicted from the stability zones of load interaction chart by Igoe & Gavin (2021), with the exception of only one point predicting pile stability incorrectly. This point (circled in red) is situated near the zone where the boundary lines converge, and where the mean cyclic load (Q_{mean}) is close to the static pile capacity. In this zone, predicting pile stability is complex due to the lines being very close together. In addition, the pile static capacity at the time of cyclic loading ($Q_{s(t)}$, calculated from the Unified CPT Method including ageing) may have an influence on the exact position of the data point. Larger pile capacities would move the point diagonally to the left and downwards, whereas smaller capacities would move the point diagonally to the right and upwards.

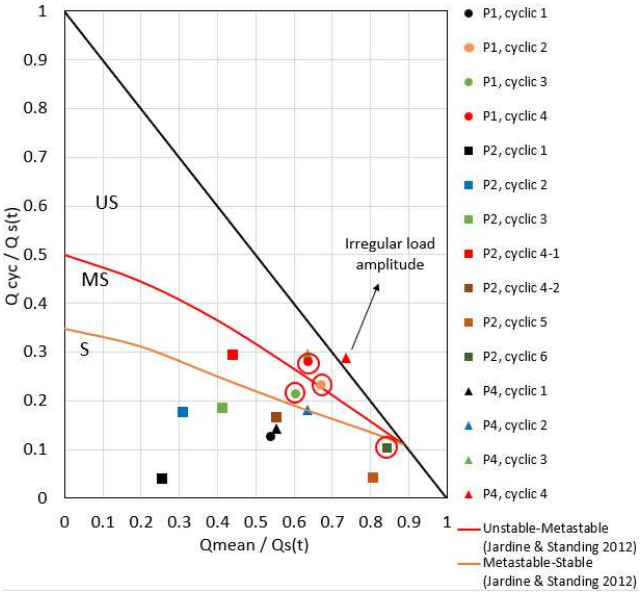

Figure 7 Predicted and observed pile stability using Jardine & Standing (2012) boundary lines

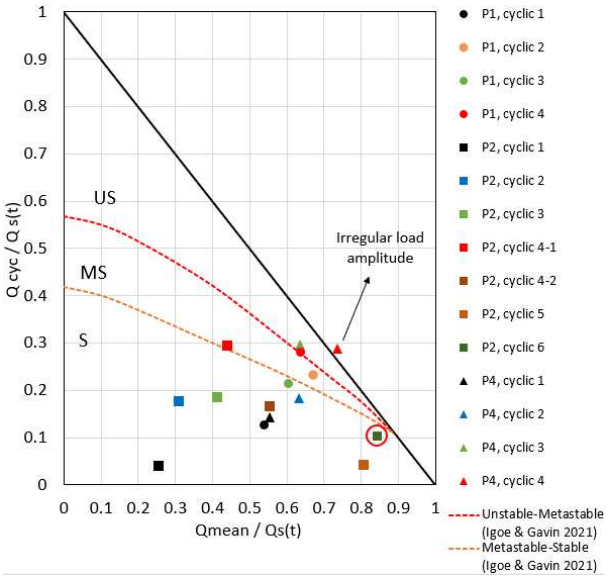

Figure 8 Prediction using Igoe & Gavin boundaries

Overall, both charts provided fairly good predictions of the stability response. Main differences in results may be attributed to differences in pile installation method (vibrated to 78 to 89% of their final tip

depths), loading frequency, saturation, pile dimensions and sand origins.

It is suggested that, for future research, more tests with cyclic loading points near the zone of convergence of the stability boundaries, i.e. with large $Q_{mean}/Q_{s(t)}$ values, are conducted to improve understanding of pile stability in that zone of the interaction charts.

Furthermore, it is worth noting that, for a certain cyclic load package, the effect of previous cyclic load packages is not considered in the analyses. Even though in most cases the cyclic load amplitude and/or mean load increased from one cyclic load package to the next ones, previous packages may have affected the pile associated static capacity for subsequent cyclic packages, whose potential effects are not covered in this paper. This may also be subject of further research.

5 CONCLUSIONS

The study compared the load interaction charts found in literature as prediction methods for assessing pile stability response under tensile cyclic loading while incorporating ageing effects into pile capacity. The following main conclusions can be drawn:

- The tension capacity developed 147 days after following a largely vibrated installation procedure is greater than the Unified CPT Method prediction.
- The interaction chart boundaries from previous literature overall align well with the pile stability results observed from the displacement accumulation in the field tests. Although the test results showed slightly better agreement with the interaction charts of Igoe & Gavin, the agreement was also fairly good with the chart of Jardine & Standing despite significant differences in loading frequency.
- To estimate pile capacity accounting for ageing, the framework proposed by Jardine & Standing (2012) was used and proved effective when combined with the interaction charts.
- There is a zone of uncertainty in the lower-right corner of the interaction charts where all the curves converge (Figure 8). Predictions in this area should be treated with caution since more data is needed to improve understanding of pile stability under the respective loading conditions.

AUTHOR CONTRIBUTION STATEMENT

A. Sharma: Data curation, Formal Analysis, Visualization, Writing- Original draft. **A. Peccin da Silva**: Writing- Reviewing and Editing, Methodology, Visualization, Formal Analysis, Supervision, Funding acquisition. **Y. Jafarian:** Data curation, Visualization, Formal Analysis. **K.G. Gavin**: Methodology, Supervision. **J. Kenkhuis:** Funding acquisition, Supervision, Field Work Team Lead. **D. de Lange**: Formal Analysis, Reviewing, Supervision.

ACKNOWLEDGEMENTS

This paper is part of the TPPT project in the framework of the GROW Research Programme. The project is funded by the Dutch Ministry of Economic Affairs and Climate Policy and TKI Offshore Energy. The authors also thank the additional financial and technical support provided by the project partners: Bluewater Energy Services, JERA, Deltares, Lloyd's Register, Single Buoy Moorings (SBM), Shell Global Solutions International, SOFEC, and TotalEnergies.

REFERENCES

Igoe, D. & Gavin, K.G. (2021). Investigation of Cyclic Loading of Aged Piles in Sand. *Journal of Geotechnical and Geoenvironmental Engineering*, 174(4): 04021011.

Gavin, K., Jardine, R.J., Karlsrud, K. and Lehane, B.M. (2015) The Effects of Pile Ageing on the Shaft Capacity of Offshore Piles in Sand (2015). Keynote paper. Proc. international Symposium Frontiers in Offshore Geotechnics (ISFOG), Oslo. June 2015, p 25.

Jardine, R.J. & Chow, F. (1996). New Design Methods for Offshore Piles, Marine Technology Directorate.

Jardine, R. Chow, F. Overy, R. and Standing, J. (2005) 'ICP Design Methods for Driven Piles in Sands and Clays', In: Thomas Telford, 105p.

Jardine, R.J. & Standing, J.R. (2012). Field axial cyclic loading experiments on driven piles in sand. *Soils and Foundations*, 54(4): 723-736.

Jardine, R.J., Standing, J.R. & Chow, F.C. (2006). Some observations of the effects of time on the capacity of piles driven in sand. *Géotechnique*, 56 (4): 227–244.

Lehane, B. Bittar, E. Liu, Z. Jardine, R. Carotenuto, P. Rattley, M. Jeanjean, P. Gilbert, R. Haavik, J. Morgan, N. Lacasse, S. and Gavin. K. (2020) A new CPT-based Axial Pile Capacity Deign method for Piles in Sand, International Symposium on Frontiers in Offshore Geotechnics, ISFOG, Austin.

Tsuha, C.H.C., Foray, P.Y., Jardine, R.J., Yang, Z.X, Silva, M. & Rimoy, S. (2012). Behaviour of displacement piles in sand under cyclic axial loading. *Soils and Foundations*, 52 (3): 393–410.